THIS IS AN EARLIER VERSION OF THE PAPER WITH DOI: 10.1109/TMTT.2018.2873335

GCPW GaAs Broadside Couplers at H-Band and Application to Balanced Power Amplifiers

Belen Amado-Rey, Yolanda Campos-Roca, Christian Friesicke, Sandrine Wagner, and Oliver Ambacher

***Abstract*—This paper reports on the first H-band broadside hybrid coupler based on a three-metallization layer process and a grounded coplanar waveguide (GCPW) environment. The performance of this integrated coupler is carefully examined through electromagnetic (EM) simulations and experimental evaluation, and compared to a tandem-X hybrid, which is based on a two-metallization layer process and requires twice the chip area. The EM analysis covers S-parameter simulations of the coupler structures as well as even- and odd-mode impedance analysis of the edge- and broadside-coupled lines. The broadside hybrid exhibits insertion losses of 3.8-4.3 dB in the through and coupled ports from 246 GHz to 297 GHz. This corresponds to a fractional bandwidth of 19 %. In this frequency range, the imbalance is lower than 0.2 dB and a phase difference of 93.6 ± 1.4° is obtained. It is demonstrated that the broadside coupler overcomes the performance of tandem-X hybrids, when applied to medium power amplifiers (MPAs). An MPA monolithic microwave integrate circuit (MMIC) based on triple stacked FETs and broadside couplers achieves at least 4.5 dBm at 300 GHz and large-signal gain of 7.5 dB at the 3 dB compression point.**

***Index Terms*—Balanced amplifier, broadside coupler, 90° coupler, metamorphic high electron mobility transistor (mHEMT), millimeter-wave monolithic integrated circuit (MMIC), power amplifier, stacked-FET, tandem-X coupler.**

I. Introduction

The development of power amplifiers with good output power, gain and bandwidth performance at millimeter-wave (mmW) and submillimeter-wave (sub-mmW) frequencies is a quite challenging task. Furthermore, as they are used for aircraft radar and imaging systems, compactness and low weight are also required. Balanced topologies are widely used to enhance the output power, as they combine two single-transistor cells in parallel. Additionally, due to the use of 90° hybrid couplers any returned mismatched signal is canceled at the input and output of the amplifier. Thus, this topology presents high input and output return losses (RLs) and it also suppress the odd-mode instabilities. An important issue is that hybrid couplers should exhibit a tight coupling ($C = 3\,\mathrm{dB}$) in the balanced amplifier, which is not possible by using edge-coupled lines alone.

Tandem-X structures can be used as hybrid couplers at mmW and sub-mmW frequencies, at which they have demonstrated good performance. As an example, a tandem-X coupler with 1.4 dB insertion loss at 320 GHz has been published in [1]. Tandem-X couplers constitute an efficient cascade combination of two identical directional couplers to solve the problem of the loose coupling provided by each single coupler. Consequently, to obtain a final 3-dB coupling, the two individual couplers have to exhibit only $C = 8.34\,\mathrm{dB}$ coupling [2]. However, tandem-X couplers require at least twice the die area of the single edge-coupled line couplers.

Another possibility to alleviate the weak coupling of the conventional edge coupled-line structure based on a grounded coplanar waveguide (GCPW) environment, is to use a broadside coupler, which is suited for tight coupling [3]. Simulation results of a broadside coupler for $150 - 240\,\mathrm{GHz}$, based on the 2-metallization layer process of the Fraunhofer Institute for Applied Solid State Physics (IAF), have been presented in [4]. A broadside coupler with branch-lines to enhance the isolation and return loss is included in [5].

The Fraunhofer IAF has recently introduced a new millimeter-wave monolithic integrated circuit (MMIC) process variant, included in the $35\,\mathrm{nm}$ gate length metamorphic high electron mobility transistor (mHEMT) technology. In comparison to the established two-layer process, this variant offers three metallization layers, which enhances compactness and design flexibility and allows the fabrication of new structures such as the broadside coupler presented here. The experimental results of this coupler demonstrate broadband performance in the H-band, concretely from 233 to $295\,\mathrm{GHz}$, and are compared to those of a tandem-X coupler. Both couplers (broadside and tandem-X) are carefully examined through electromagnetic (EM) simulations of the even- and odd-mode impedances and S-parameters of the whole coupler structures. In addition, two identical medium power amplifiers (MPAs) have been realized using the tandem-X and broadside GCPW couplers. These MPAs include two triple stacked-FET transistor cells in a balanced topology to enhance the output power.

The paper is organized as follows: In Section II, a description of the technology is included. Section III covers even- and odd-mode analysis of the edge and broadside coupled lines. In Section IV and V, respectively, the design and measurements of the tandem-X and broadside couplers are included. Section VI compares the performance of both hybrid couplers and Section VII includes MPA realizations based on them. Finally, the conclusions of this work are summarized in Section VIII.

II. Technology

The technology used in the MMICs is based on InGaAs/InAlAs mHEMT heterostructures on 4” semi-insulating

B. Amado-Rey is with the Institute of Microsystem Techniques, Albert-Ludwigs-University Freiburg, Germany. E-mail: aamadore@alumnos.unex.es

C. Friesicke, S. Wagner and O. Ambacher are with the Fraunhofer Institute for Applied Solid State Physics IAF, 79108 Freiburg, Germany.

Y. Campos-Roca is with the Department of Computer and Communication Technologies, University of Extremadura, 10003 Caceres, Spain.

Manuscript received XX, XXXX; revised XX, XXXX.

TABLE I
ELECTRICAL DC- AND RF-PARAMETERS OF THE 35 NM MHEMT PROCESS ($W_G = 2 \times 10$ μm).

Parameter	Symbol	Unity	Values
Indium content of composite channel	In	%	80
Transit frequency	f_T	GHz	515
Max. osc. frequency	f_{max}	GHz	1000
Max. transconductance	$g_{m,max}$	mS/mm	2500
Max. drain current density	$I_{d,max}$	mA/mm	1600
Off-state breakdown voltage	$BV_{\text{off-state}}$	V	2
On-state breakdown voltage	$BV_{\text{on-state}}$	V	1.5

GaAs substrates, using T-gates with a length of 35 nm. To adapt the lattice constant, the buffer is graded so that the $Al_{0.52}Ga_{0.48}As$ (GaAs) layer is linearly exchanged to $Al_{0.52}In_{0.52}As$ (InAs). This metamorphic buffer is placed between the GaAs substrate at the bottom and the InGaAs channel beneath the T-shaped gate contact [6]. A Pt-Ti-Pt-Au layer sequence is used for gate metallization. To suppress substrate modes, the wafers are thinned down to 50 μm.

As shown in Table I, the 35 nm gate-length technology features a channel indium content of 80 %, and the transit frequency (f_T) and maximum oscillation frequency (f_{max}) are 515 GHz and 1 THz, respectively [7]. These high frequencies are suitable for the design of MMICs in the sub-mmW frequency range. Moreover, a transconductance of $g_{m,max} = 2500\,\mathrm{mS/mm}$ and a maximum drain current of $I_{DS,max} = 1600\,\mathrm{mA/mm}$ are achieved for a common-source (CS) transistor with a total gate width (W_G) of 2×10 μm. The off-state breakdown voltage is $BV_{off-state} = 2\,\mathrm{V}$.

The MMICs processed in this work are based on a three-metallization layer process. This process allows the use of three top metal stacked-layers (MET1, MET2, METG). MET1 and MET2 are electron evaporated Au layers with the same 0.3 μm thickness, while METG is an Au layer produced by galvanic metallization and has a thickness of 2.7 μm. This galvanic layer is also used to implement air-bridges that interconnect the top ground metal layers and, consequently, avoid the propagation of the undesired slot-line mode.

In comparison to the two-layer process shown in Fig. 1, which is explained in detail in [8], the three-layer technology adds a second benzocyclobutene (BCB) layer (BCB2) between MET1 and MET2 (see Fig. 2). This new BCB layer and the addition of MET2 (the two-layer process includes only MET1 and METG) increases the degree of design flexibility and allows for new and more compact structures such as the broadside coupler represented in Fig. 2.

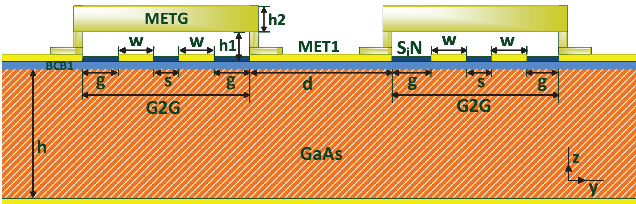

Fig. 1. Cross-sectional view of the GCPW tandem-X coupler.

Another important characteristic of the three-layer process is the thickness reduction of the SiN layer compared to the two-layer process. Hence, in the two-layer process the capacitance value per area is $0.225\,\mathrm{fF/\mu m^2}$, whereas in the three-layer process is $0.8\,\mathrm{fF/\mu m^2}$. Then, less die area is needed to achieve the same capacitance value, resulting in more compactness.

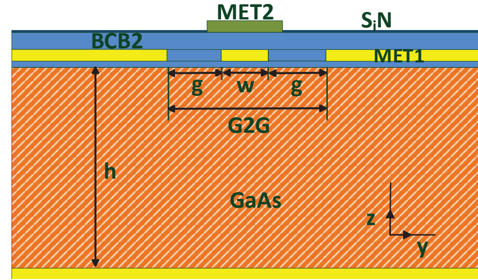

Fig. 2. Cross-sectional view of the GCPW broadside coupler.

III. COMPARATIVE ANALYSIS OF EDGE- AND BROADSIDE-COUPLED LINES

When two metal strips are placed close to each other, a certain amount of EM-field energy is transferred from one line to the other, which is quantified through the coupling factor (C). The value of C for the coupled lines depends on design parameters such as the width of the parallel metal strips (w), the spacing between them (s) and the ground-to-ground (G2G) separation in the GCPW environment.

A structure with two grounded-coupled lines supports two propagation modes: even and odd. When the coupled lines are excited through an input signal, their maximum C value for a quarter wavelength ($\lambda/4$) can be described as a relation between the modes [9]:

$$C = \frac{Z_{0e} - Z_{0o}}{Z_{0e} + Z_{0o}}, \tag{1}$$

where Z_{0e} and Z_{0o} are the characteristic impedances of the even and odd modes, respectively.

A. Design parameters of edge- and broadside-coupled lines

The tandem-X (see Fig. 1) and broadside couplers (see Fig. 2) described in this paper are based on edge- and broadside-coupled lines, respectively, whose design parameters are included in Table II. In order to evaluate the influence of these parameters in the C values, coupling error and bandwidth, as well as phase quadrature, two different geometries for each coupled-line type are investigated.

TABLE II
GEOMETRY PARAMETERS FOR THE EDGE- AND BROADSIDE-COUPLED LINES OPERATING AT 300 GHZ.

Geometry parameters	Edge lines 1	Edge lines 2	Broadside lines 1	Broadside lines 2
G2G (μm)	23.6	41.6	21.6	21.6
g (μm)	3.3	6.5	7	7
w (μm)	7.4	12	7.6 (MET1) 6.4 (MET2)	7.6 (MET1) 6.4 (MET2)
s (μm)	2.2 (air)	4.6 (air)	1.4 (BCB2)	1.4 (BCB2)
Length (μm)	115	115	L_{11}=L_{21}=115	$L_{12} = 108$ $L_{22} = 140$

As shown in Figs. 1 and 2, the parameter s included in Table II indicates the spacing between the two metal strips that are producing the coupling in each case. For the edge-coupled lines it is the horizontal distance between the two MET1 strip lines, whereas for the broadside-coupled lines this space is equivalent to the BCB2 layer thickness (vertical distance between MET1 and MET2 strips).

The dimensions g, w and s of the four coupled-lines are obtained through EM optimizations of the even- and odd-mode impedances, performed in CST Microwave Studio. First, a fixed odd-mode impedance is determined by w. Then, the even-mode impedance is optimized by tuning s and g to achieve the best feasible coupling and bandwidth in a $50\,\Omega$ GCPW environment. In addition, the length corresponds to $\lambda/4$ at the design target frequency of 300 GHz. L_{11}, L_{12}, L_{21} and L_{22} correspond to the MET1 and MET2 lengths for the two broadside-couple-line configurations, as shown in Fig. 3.

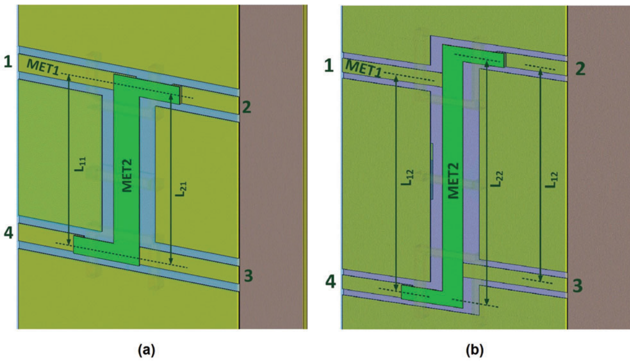

Fig. 3. EM models of (a) Broadside coupler 1 and (b) Broadside coupler 2.

B. Even- and odd-mode analysis through EM simulations

By using a multiport simulation in CST, the common- and differential-mode impedances for the four coupled-lines in Table II are simulated. From them, Z_{0e} and Z_{0o} are determined. These impedances, as well as the coupling factors obtained by applying (1), are included in Table III. This table also shows the coupler impedance (Z_C), calculated from the even- and odd-mode impedances by applying $Z_C = \sqrt{Z_{0e} \cdot Z_{0o}}$.

It is observed that the edge-coupled lines 1 achieve C=8.6 dB, whereas a better coupling factor, C=8.4 dB, is obtained in the case of the edge-coupled lines 2. This means that a coupling error between S_{21} and S_{31} of 0.4 dB is expected when using the edge-coupled lines 2 to develop the Tandem-X coupler 2, whereas almost no coupling error is expected when using the edge-coupled lines 1. Also, the coupler impedance calculated for edge-coupled lines 2 (see Table III) is closer to $50\,\Omega$ than in the case of edge-coupled lines 1, which leads to a better return loss performance and lower insertion losses. Thus, the dimensions of the edge-coupled lines 2 are chosen to develop the Tandem-X coupler 2.

TABLE III
EXTRACTED EVEN- AND ODD-MODE CHARACTERISTIC IMPEDANCES, COUPLER IMPEDANCE AND COUPLING FACTOR AT 300 GHz.

Coupled-line topology	$Z_{0e}(\Omega)$	$Z_{0o}(\Omega)$	$Z_C(\Omega)$	$C(dB)$
Edge-coupled lines 1	101.4	46.5	68.7	8.6
Edge-coupled lines 2	69.2	31.0	46.3	8.4
Broadside-coupled lines	95.4	18.5	42	3.4

Instead, the even- and odd-mode impedance difference for the broadside coupler lines differ more strongly, leading to a tighter coupling factor of $C = 3.4$ dB. Thus, it is verified that the broadside-coupled lines are well suited for tight coupling and constitute by themselves a good 3-dB hybrid coupler, without the need of a tandem configuration. Concerning the coupler impedance ($42\,\Omega$), the matching to $50\,\Omega$ is slightly worse than in the case of edge-coupled lines 2, but still sufficient to achieve usable return loss values. By performing simulations of ideal coupled lines in ADS, return losses of 23.7 dB and 20.4 dB are obtained for coupler impedances of $46.3\,\Omega$ and $42\,\Omega$, respectively.

IV. TANDEM-X COUPLER

The tandem-X coupler described in this section is developed by using two cascaded edge-coupled lines 2. This structure has been 3D EM simulated by using CST Microwave Studio, and was afterwards processed and measured.

A. Design description

The schematic cross-sectional view of the Tandem-X coupler 2 is illustrated in Fig. 1, whose parameters correspond to the values of the edge-coupled lines 2 included in Table II. Thus, the coupling is produced horizontally between the two MET1 strips, separated by a distance of $s = 4.6$ µm.

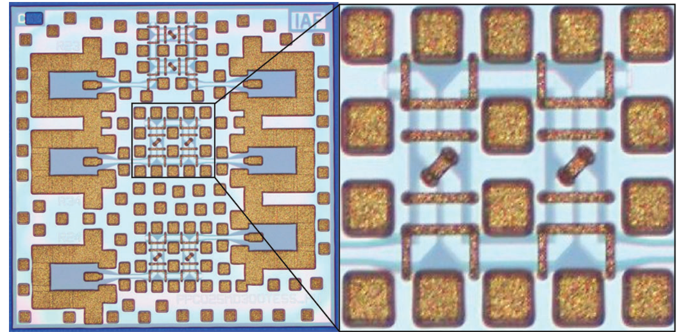

Fig. 4. Chip photograph of the processed Tandem-X coupler 2.

The chip photograph of the Tandem-X coupler 2 is shown in Fig. 4, where three configurations of the same coupler are included to measure coupling, direct transmission and isolation. The die size per coupler without taking into account the RF pads and the de-embedding lines is 0.16x0.22 mm^2. Both RF pads and GCPW lines are de-embedded by using the short-open-load-reciprocal-thru (SOLR) algorithm.

B. Measurement results

The measured and simulated results of the processed Tandem-X coupler 2 are shown in Fig. 5, achieving a very good agreement. The measured symmetric bandwidth that includes the two frequencies for which $|S_{21} - S_{31}| = 0$ is extended from 249 to 296 GHz (fractional bandwidth, $FBW = 17\,\%$). In this bandwidth, the measured insertion losses (ILs) are 3.8-4.6 dB and the isolation (S_{41}) is better than 25 dB. Note that this IL definition refers to the ratio of the output power at the thru and coupled ports to the power at

the input port. Ideally this is $3\,\mathrm{dB}$. In addition, the difference between the coupled and direct port is less than $0.7\,\mathrm{dB}$ in the considered FBW. The measured phase difference between the direct and the coupled ports is quite broadband, with an average value of $92°$ and a variation of $\pm 2°$ over the FBW.

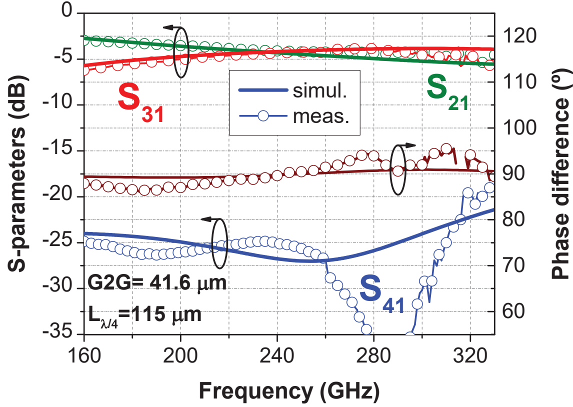

Fig. 5. EM simulated and measured S-parameters and phase difference for the Tandem-X coupler 2.

V. Broadside coupler

For the broadside coupler in the 3-layer technology, as the dielectric that separates MET1 and MET2 is BCB2 instead of air, a tight coupling of around $3\,\mathrm{dB}$ is feasible. The design and de-embedded measurement results of this coupler are described in this section.

A. Design description

As shown in Fig. 2, the 3-layer broadside coupler uses two identical $0.3\,\mu\mathrm{m}$ metallization layers (MET1 and MET2), which constitute the coupled lines. They are separated by a $1.4\,\mu\mathrm{m}$ BCB layer, which acts as the dielectric (instead of air between MET1 and METG as in [4]).

In this case, broadside-coupled lines constitute an asymmetric structure where the coupling coefficient is much stronger than for the edge-coupled lines due to the close proximity between MET1 and METG. This is a result of the BCB2 layer, which is thinner than the minimum gap realizable between edge-coupled lines. This strong coupling produces a wider bandwidth than in the case of edge-coupled lines. As the GCPW is not a homogeneous environment and because of the asymmetry of the metallization lines that constitute the broadside coupler [10], simplified equations to determine the even- and odd-mode impedances cannot be applied. Thus, to perform the design, the hybrid is EM modeled in CST. The strip widths (for MET1 and MET2) and the G2G separation are optimized within CST to obtain the mode impedances required to achieve a $3\,\mathrm{dB}$ coupling. Theoretically, the length is $\lambda/4$ at the frequency of interest ($300\,\mathrm{GHz}$ in this case).

The broadside coupler has been designed using the parameters extracted from the optimization, which are included in Table II. The final EM model of the broadside coupler is shown in Fig. 3 (a). It can be observed that both metal layers MET1 and MET2 are coupled to each other, whereas the input and output signals are transmitted and received at the ports by using MET1. The electrical asymmetry in the structure results in a poor phase behaviour.

To deal with this issue, another broadside coupler (see Fig. 3 (b)) has been designed, EM simulated and processed. The optimized physical length of the coupled MET2 layer (L_{22}) is larger than MET1 (L_{12}) to reduce that phase difference. This large phase difference is due to the fact that the coupled metal strip lines are in an inhomogeneous medium (the respective dielectrics are GaAs and BCB) and then, strongly different phase propagation constants for the even- and odd-modes are produced [11]. The best simulated performance was obtained for $L_{12} = 108\ \mu\mathrm{m}$ and $L_{22} = 140\ \mu\mathrm{m}$.

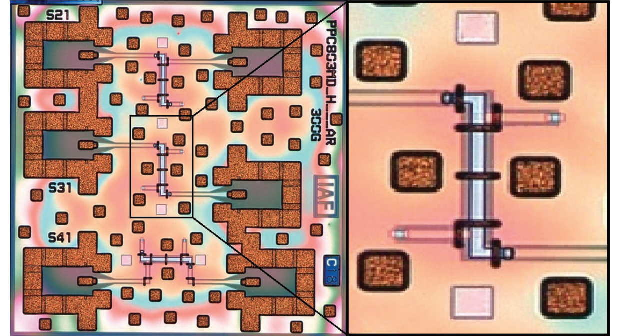

Fig. 6. Chip photograph of Broadside coupler 2.

The photograph of the processed MMIC is shown in Fig. 6, where three test broadside coupler structures to measure S_{21}, S_{31} and S_{41} parameters are placed. The die size per coupler without taking into account the RF pads and the de-embedding lines is $0.08\mathrm{x}0.22\,\mathrm{mm}^2$. In comparison to the Tandem-X coupler 2, this means a size reduction by a factor of 2.

B. Measurement results

The measurement-simulation comparison of Broadside coupler 1 is presented in Fig. 7, with a good agreement. The measured IL is $4.3 - 4.6\,\mathrm{dB}$ from $271\,\mathrm{GHz}$ to $293\,\mathrm{GHz}$ (FBW=$8\,\%$). Apart from the narrow bandwidth and high losses, the phase difference between ports 2 and 3 is not close to $90°$ but, instead, it varies from $76°$ to $85°$ in the measured range (200-335 GHz). This poor phase behavior is a result of the electrical asymmetry in the structure.

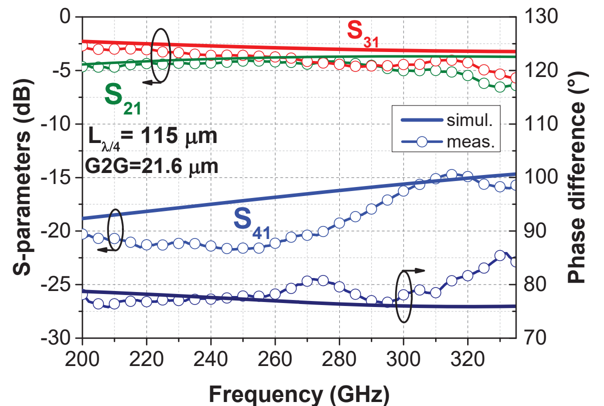

Fig. 7. Measured and EM simulated results of the Broadside coupler 1.

TABLE IV
H-BAND STATE-OF-THE-ART COUPLERS. FOR [12] AND [1] THE VALUES CORRESPOND TO THE 0.5 dB BANDWIDTH (FBW) WHERE $RL > 13$ dB.

Coupler type	Reference	IL (dB)*	Bandwidth (GHz)	Isolation (dB)	Coupling error (dB)	Phase difference	Size (mm^2)
Branch-line	[12]	3.6-4.5	210-280 (29 %)	NA	NA	NA	NA
Tandem-X	[1]	4.2-4.8	220-320 (37 %)	NA	NA	NA	NA
Tandem-X	**Tandem coupler 2**	3.8-4.6	249-296 (17%)	> 25	<0.7	$92 \pm 2^{\circ}$	0.16×0.22
Broadside	**Broadside coupler 2**	3.8-4.3	246-297 (19 %)	> 17	<0.2	$93.6^{\circ} \pm 1.4^{\circ}$	0.08×0.22

* It refers to both thru and coupled ports.

The simulated and measured S-parameters of the Broadside coupler 2 are plotted in Fig. 8. The measured performance is summarized in Table IV. A best coupling of 3.8 dB is achieved at 266 GHz and the complete bandwidth for which $|S_{21} - S_{31}| < 0.2$ dB (only 0.2 dB of coupling error) is extended from 246 GHz to 297 GHz. The measured ILs in this range are $3.8 - 4.3$ dB.

An average value of the phase difference of 93.6° with small variations of $\pm 1.4^{\circ}$ is achieved by this broadside hybrid in the considered symmetric bandwidth and the isolation presents higher values than 17 dB.

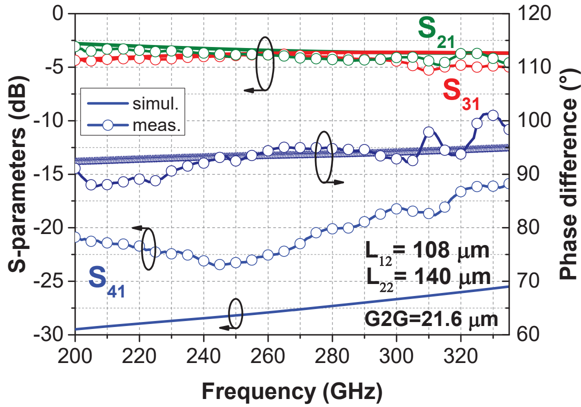

Fig. 8. Measured and EM simulated results of the Broadside coupler 2.

VI. TANDEM-X AND BROADSIDE COUPLERS COMPARISON

In comparison to the Tandem-X coupler 2, the Broadside coupler 2 reduces the maximum insertion losses (see Table IV) and exhibits a higher bandwidth with reduced coupling error. Thus, for the Broadside coupler 2 an excellent coupling error better than 0.2 dB is obtained over a 19 % FBW. The reduction in size is also accomplished, as the Broadside coupler 2 reduces by half the die size of Tandem-X coupler 2. To the best of the authors' knowledge, this is the first Broadside coupler whose measurements are demonstrated in this frequency range. In [4] only the simulated performance is depicted from 150 GHz to 240 GHz.

Looking at Table IV it can be stated that the lowest maximum IL is achieved by the novel Broadside coupler 2, fabricated using the 3-layer technology, even when comparing it with the state-of-the art hybrids in [1] and [12]. Also, a high isolation (> 17 dB) within a quite wide bandwidth of 51 GHz is performed by this structure. Although the bandwidth of the tandem-X coupler in [1] and the branch-line coupler in [12] is wider, several performance parameters of these couplers are not available as they measured them through a back-to-back configuration. Moreover, the FBW has not been defined by the frequencies where the two coupling parameters intersect ($|S_{21} - S_{31}| = 0$), but considering a 0.5 dB bandwidth and $RL > 13$ dB. The bandwidth of the Broadside coupler 2 is enlarged to 23 % (from 233 GHz to 295 GHz), when defining it as in [1] and [12]. In addition, the tandem-X and Branch-line couplers have a large die area which is problematic for very compact designs.

VII. MPAS BASED ON TANDEM-X AND BROADSIDE COUPLERS

The performance of the Broadside coupler 2 is compared to the tandem-X coupler 2 through the realization of two identical balanced MPAs at 300 GHz, where only the couplers are changed.

A. Design description

The triple stacked-FET cells which constitute the balanced MPAs are illustrated in Fig. 9. The triple stacked configuration is based on a 4×10 µm CS transistor connected in series to two 4×10 µm common-gate like transistors, whose gates are not RF grounded with the aim of enhancing the final output power. Therefore, the capacitor values are $C_1 = 371$ fF and $C_1 = 491$ fF. Due to stability issues, GCPW lines are included between the transistors, as shown in Fig. 9 (b). This topology is explained in detail in [13].

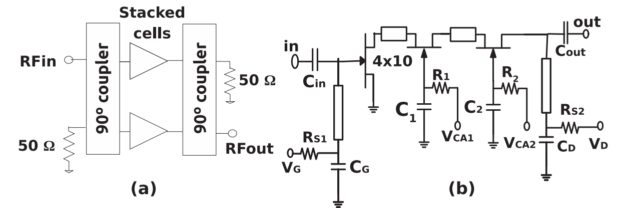

Fig. 9. Schematic diagram of (a) the balanced MPAs and (b) a single stacked-FET cell of the MPAs.

The chip photographs of the processed MPAs that use either tandem-X or broadside couplers are shown in Figs. 10 and 11, respectively. Both circuits are designed with the same area of $1.5 \times 0.75\,\text{mm}^2$ to do a fair comparison. However, the die area of the MPA containing the Broadside coupler 2 can be reduced.

B. Measurements and discussion

The simulated and measured small-signal results of both MMICs are depicted in Figs. 12 and 13, respectively. An Agilent N5224A vector network analyzer system with two Oleson V03VNA2 T/R frequency extension modules and two Picoprobe Infinity GSG 60 microwave probes are used for the

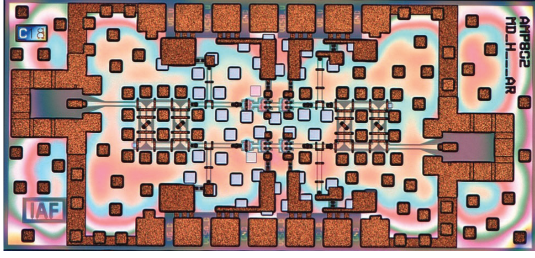

Fig. 10. Balanced MPA containing two parallel triple stacked-FETs and two tandem-X hybrids 2 (MPA1).

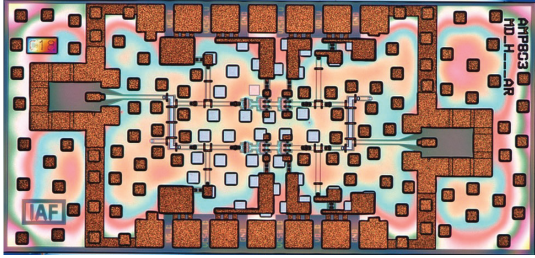

Fig. 11. Balanced MPA containing two parallel triple stacked-FETs and two Broadside couplers 2 (MPA2).

S-parameter measurements. The RF close pads and GCPW lines are de-embedded with the SOLR algorithm. The applied bias condition is as follows: $V_G = 0.12$ V, $V_{CA1} = 1.12$ V, $V_{CA2} = 2.12$ V and $V_D = 3.0$ V.

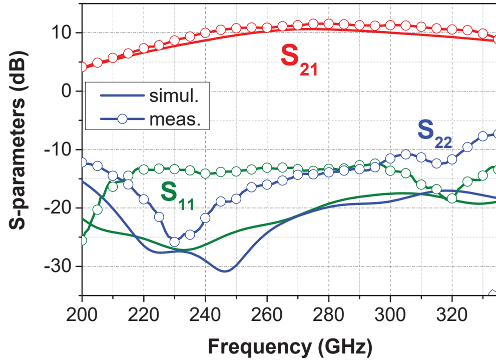

Fig. 12. Measured and simulated S-parameters of MPA1.

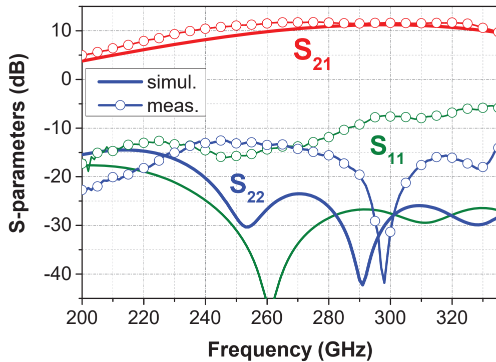

Fig. 13. Measured and simulated S-parameters of MPA2.

In Fig. 12 (MPA1), a peak gain of 11.6 dB is obtained at 278 GHz, with a 0.5 dB bandwidth from 265 GHz to 308 GHz ($FBW = 15$ %). Similarly, a maximum small-signal gain of 11.6 dB is observed for the MPA2 in Fig. 13 at 298 GHz, however the bandwidth is wider, since it extends between 251 and 326 GHz (FBW=26 %). The lack of a stacked-FET model leads to the measurement-simulation magnitude difference seen in S_{11}.

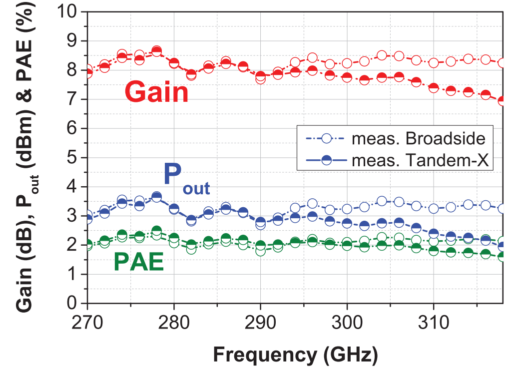

Fig. 14. Frequency sweep for P_{in}=−5 dBm for both MPAs.

The large-signal results are obtained by using a scalar measurement system, based on an H-band Erickson power sensor. For the same bias points as in the S-parameter measurements, MPA2 (with broadside couplers) exhibits a wider bandwidth than MPA1 (with tandem-X couplers), as depicted in Fig. 14. For an input power of −5 dBm higher output power levels than 3.3 dBm (around 3 dB in compression) are measured from 294 GHz to 318 GHz for MPA2. The gain and power added efficiency (PAE) in this range present values that exceed 8.2 dB and 2.1 %, respectively. However, at the same frequency range and input power level, MPA1 exhibits better power levels than 1.9 dBm. Its gain and PAE in that range exceed 6.9 dB and 1.6 %, respectively.

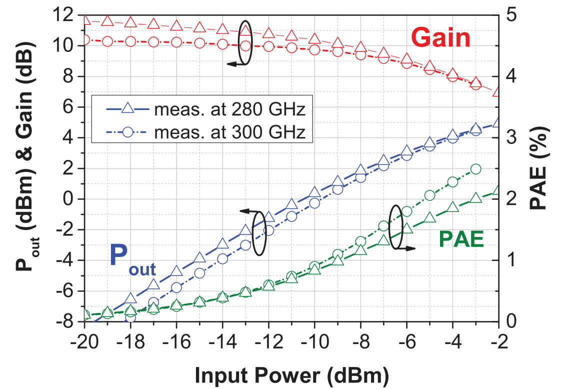

Fig. 15. P_{in} sweep for MPA2 at two frequencies.

Finally, the input power sweep for the MPA with the broadside couplers is included in Fig. 15 at two frequencies. It is seen that the compression is lower at 300 GHz than at 280 GHz. The maximum measured output power at 300 GHz is 4.5 dBm, with $PAE = 2.5$ % and large signal gain of 7.5 dB at the 3 dB compression point. The amplifier is not in saturation. Hence, higher output power levels are expected.

VIII. Conclusion

In this paper, the first GCPW broadside coupler based on a 3-metallization layer process in H-band has been demon-

strated. An excess IL that is lower than 1.3 dB and a coupling error than is lower than 0.2 dB is simultaneously achieved between 246 GHz and 297 GHz (FBW=19 %). It has been demonstrated that an MPA based on this broadside coupler obtains a wider power bandwidth with higher power levels than when using tandem-X couplers. This MPA has achieved a maximum output power of 4.5 dBm at 300 GHz in a balanced configuration of two triple- stacked FET cells. Apart from that, the broadside coupler size reduction is also remarkable, achieving a factor of two smaller layout area than for the tandem-X structure.

ACKNOWLEDGMENT

The authors would like to thank M. Cwiklinski for his good advice about the phase issue in the broadside coupler, and the Fraunhofer IAF staff for their excellent contribution done during model development as well as epitaxial growth and wafer processing, concretely Dr. A. Leuther. Furthermore, they would like to thank Dr. J. Kühn, Dr. M. Schlechtweg and Dr. F. van Raay for their continuous support throughout this work.

REFERENCES

[1] V. Radisic, W. R. Deal, K. M. K. H. Leong, X. B. Mei, W. Yoshida, P. H. Liu, J. Uyeda, A. Fung, L. Samoska, T. Gaier, and R. Lai, "A 10-mW submillimeter-wave solid-state power-amplifier module," *IEEE Trans. Microw. Theory Techn.*, vol. 58, no. 7, pp. 1903–1909, July 2010.

[2] J.-H. Cho, H.-Y. Hwang, and S.-W. Yun, "A design of wideband 3-dB coupler with N-section microstrip Tandem structure," *IEEE Microw. Compon. Lett.*, vol. 15, no. 2, pp. 113–115, Feb 2005.

[3] R. Simons, *Coplanar Waveguide Circuits, Components, and Systems*, ser. Wiley Series in Microwave and Optical Engineering. Wiley, 2004.

[4] J. Längst, S. Diebold, H. Massler, A. Tessmann, A. Leuther, T. Zwick, and I. Kallfass, "A balanced 150-240 GHz amplifier MMIC using airbridge transmission lines," *INMMIC Workshop*, pp. 1–3, Sept 2012.

[5] Y. S. Noh, M. S. Uhm, and I. B. Yom, "LTCC Broadside Coupler Design with Branch Lines for Enhanced Performances," in *2007 MTT-S Int. Microw. Symp. Dig.*, June 2007, pp. 1015–1018.

[6] D. Lopez-Diaz and O. Ambacher, *Broadband Transceiver Circuits for Millimeter-Wave Wireless Communication*, ser. Science for Systems. Fraunhofer Verlag, 2015.

[7] F. Thome, A. Leuther, H. Massler, M. Schlechtweg, and O. Ambacher, "Comparison of a 35-nm and a 50-nm gate-length metamorphic HEMT technology for millimeter-wave low-noise amplifier MMICs," *IEEE MTT-S Int. Microw. Symp. Dig.*, pp. 752–755, June 2017.

[8] B. Amado-Rey, Y. Campos-Roca, R. Weber, S. Maroldt, A. Tessmann, H. Massler, S. Wagner, A. Leuther, and O. Ambacher, "Impact of metallization layer structure on the performance of G-Band branch-line couplers," *IEEE Microw. Compon. Lett.*, vol. 25, no. 12, pp. 793–795, Dec 2015.

[9] A. Grebennikov, "Power combiners, impedance transformers and directional couplers: part IV," *HF Electronics*, pp. 18–24, March 2008.

[10] G.-H. Ryu, D.-H. Kim, J.-H. Lee, and K.-S. Seo, "A novel 3-dB coupler for MMIC using air-gap stacked microstrip lines," *IEEE Microw. Guided Lett.*, vol. 10, no. 1, pp. 1–3, Jan 2000.

[11] F. Tefiku, E. Yamashita, and J. Funada, "Novel directional couplers using broadside-coupled coplanar waveguides for double-sided printed antennas," *IEEE Trans. Microw. Theory Techn.*, vol. 44, no. 2, pp. 275–282, Feb 1996.

[12] V. Radisic, D. Scott, A. Cavus, and C. Monier, "220-GHz high-efficiency InP HBT power amplifiers," *IEEE Trans. Microw. Theory Techn.*, vol. 62, no. 12, pp. 3001–3005, Dec 2014.

[13] B. Amado-Rey, Y. Campos-Roca, F. van Raay, C. Friesicke, S. Wagner, H. Massler, A. Leuther, and O. Ambacher, "Analysis and development of submillimeter-wave stacked-FET power amplifier MMICs in 35-nm mHEMT technology," *IEEE Trans. THz Sci. Technol.*, no. 99, pp. 1–8, Feb 2018.

Ana Belén Amado Rey was born in Cáceres, Spain, in 1989. She received the Dipl.-Ing. degree and Master degree in Telecommunication Engineering from the University of Extremadura, Cáceres, Spain, in 2010 and 2014, respectively. From 2014 to 2018 she was at the Fraunhofer Institut für Angewandte Festkörperphysik (IAF) working on the design of millimeter-wave frequency power amplifiers using GaAs mHEMT technology. She is currently pursuing the Ph. D. degree based on the same topic at the Albert-Ludwigs-University in Freiburg.

Yolanda Campos-Roca was born in Guitiriz (Lugo), Spain, in 1970. She received the Dipl.-Ing. degree and Ph. D. degree in Telecommunication Engineering from the University of Vigo, Vigo, Spain, in 1994 and 2000, respectively. Her Ph. D. dissertation concerned the design of millimeter-wave frequency multipliers. From 1996 to 2000 she realized several stays at the Fraunhofer IAF, Freiburg, Germany, either as a guest researcher or as a staff member. In 2000, she joined the University of Extremadura (Spain), as an Assistant Professor, and in 2002, she became an Associate Professor. Her main research interests are in the area of MMIC design in the millimeter-wave range.

Christian Friesicke (S'07–M'15) was born in Berlin, Germany, in 1981. He received the Dipl.-Ing. degree in Electrical Engineering from the Technische Universität Hamburg-Harburg, Hamburg, Germany, in 2008.

From 2005 to 2006, he was a Visiting Scholar at the University of California at Berkeley, USA. From 2008 to 2015, he was with the Institut für Hochfrequenztechnik, Technische Universität Hamburg-Harburg, Hamburg, Germany. In 2015, he joined the Fraunhofer Institute for Applied Solid State Physics IAF in Freiburg, Germany, where he is involved in the MMIC design activities. His current research interests are the theory and design of power amplifiers in III-V and GaN technologies.

Sandrine Wagner received a Bachelor of Science in Electronics and Informatics from the University of Mulhouse, France in 1989. She joined Micronas GmbH in Freiburg, Germany in 1989 where she was responsible for layout and physical verification of large scale integrated semi-conductor devices. In 2010 she joined the measurement technology group at Fraunhofer Institute for Applied Solid State Physics (IAF), Freiburg, Germany.

Oliver Ambacher received his Dipl.-Phys. and Dr. degrees with honors from the Ludwig-Maximilians and Technical University Munich, in 1989 and 1993, respectively. In 1993, he joined the Walter Schottky Institute of the TU-Munich. 1998/99, he spent one year at Cornell University, Ithaca, NY, as an Alexander von Humboldt fellow. He became a Professor of Nanotechnology and head of the Institute for Solid State Electronics, Technical University of Ilmenau, in 2002. In 2007 he became the head of the Fraunhofer IAF and Professor for Compound Microsystems in Freiburg, Germany. Since 2017 he holds the Chair of Power Electronic at the Institute for Sustainable System Engineering belonging to the University Freiburg.